Ionospheric longitudinal variations at midlatitudes: Incoherent scatter radar observation at Millstone Hill

SCIENCE CHINA
Technological Sciences

May 2012 Vol.55 No.5: 1153–1160
doi: 10.1007/s11431-012-4784-y

Ionospheric longitudinal variations at midlatitudes: Incoherent scatter radar observation at Millstone Hill

ZHANG ShunRong*, COSTER Anthea, HOLT John, FOSTER John & ERICKSON Phil

MIT Haystack Observatory, Off Route 40, Westford, MA 01866, USA

Received January 2, 2012; accepted February 9, 2012; published online March 26, 2012

Incoherent scatter radar (ISR) extra-wide coverage experiments during the period of 1978–2011 at Millstone Hill are used to investigate longitudinal differences in electron density. This work is motivated by a recent finding of the US east-west coast difference in TEC suggesting a combined effect of changing geomagnetic declination and zonal winds. The current study provides strong supporting evidence of the longitudinal change and the plausible mechanism by examining the climatology of electron density *Ne* on both east and west sides of the radar with a longitude separation of up to 40^{o} for different heights within 300–450 km. Main findings include: 1) The east-west difference can be up to 60% and varies over the course of the day, being positive (East side *Ne* > West side *Ne*) in the late evening, and negative (West side *Ne* > East side *Ne*) in the pre-noon. 2) The east-west difference exists throughout the year. The positive (relative) difference is most pronounced in winter; the negative (relative) difference is most pronounced in early spring and later summer. 3) The east-west difference tends to enhance toward decreasing solar activity, however, with some seasonal dependence; the enhancements in the positive and negative differences do not take place simultaneously. 4) Both times of largest positive and largest negative east-west differences in *Ne* are earlier in summer and later in winter. The two times differ by 12–13 h, which remains constant throughout the year. 5) Variations at different heights from 300–450 km are similar. Zonal wind climatology above Millstone Hill is found to be perfectly consistent with what is expected based on the electron density difference between the east and west sides of the site. The magnetic declination-zonal wind mechanism is true for other longitude sectors as well, and may be used to understand longitudinal variations elsewhere. It may also be used to derive thermospheric zonal winds.

midlatitude ionosphere, geomagnetic declination, thermospheric zonal winds, longitudinal variation, incoherent scatter radar

Citation: Zhang S R, Coster A J, Holt J M, et al. Ionospheric longitudinal variations at midlatitudes: Incoherent scatter radar observation at Millstone Hill. Sci China Tech Sci, 2012, 55: 1153–1160, doi: 10.1007/s11431-012-4784-y

1 Introduction

Ionospheric longitudinal variations show different characteristics with latitudes. For equator and low latitudes, there exists a wave-4 structure at a fixed local time (see ref. [1, 2] for initial results). This planetary-scale phenomenon is mainly associated with electric fields generated by nonmigrating atmospheric tides in the E-region height that vary with longitude [3]. At midlatitudes, some longitudinal variations, such as those in annual and semi-annual ionospheric changes, have been explained as the result of the separation of geographic and geomagnetic poles and the associated distance from the aurora zone at different longitude sectors [4].

Using GPS Total Electron Content (TEC) observations

*Corresponding author (email: shunrong@haystack.mit.edu)

made by a network of dense GPS receivers over the continental US, we have uncovered a new phenomenon of US east-west coast ionospheric differences [5]. The evening TEC is substantially higher on the US east coast than on the west, and vice versa for the morning TEC; the longitudinal difference displays a clear diurnal variation. Through an analysis of morning-evening variability in the east-west TEC difference, minimum variability is found to coincide with the longitudes of zero magnetic declination over the continental US. It was suggested that these new findings of longitudinal differences in ionospheric TEC at midlatitudes are caused by the longitudinal difference in magnetic declination combined with the effect of thermospheric zonal winds, which are subject to directional reversal over the course of a day. GPS TEC data provide ionospheric electron density information in an integrated sense, while detailed information on height variations and full climatology including seasonal and solar cycle dependency, which can be equally or more compelling from the point of view of physical understanding, may be obtained with other means of observations, such as incoherent scatter radars (ISRs).

In this present study, we use ISR long-term observations over Millstone Hill (42.5°N, 288.6°E) to investigate longitudinal differences of electron density at various heights. This has been feasible since the radar, with a fully steerable antenna (in addition to the fixed zenith antenna), can provide an extra wide coverage with a longitude span from approximately −45 to −95°E depending on the antenna's elevation, and a height span up to a few hundreds of kilometers. The long-term database allows for determination of seasonal and solar cycle dependency. In the following sections, we start with a brief description of the observation and datasets, and then we describe methodology of data processing. We present diurnal, seasonal, solar cycle, and height dependency of the longitudinal variation in Result section. In Discussion section, we address a comparison between our results and the Weddell Sea anomaly, another midlatitude ionospheric characteristic of evening electron density enhancement, the zonal wind climatology and implication of this study. The final section provides a summary of the main findings.

2 Observation

The Millstone Hill UHF incoherent scatter radar system operates with a zenith-directed 68-m diameter fixed parabolic antenna, which commenced operation in 1963. This provides vertical measurements of the upper atmosphere up to 1000 km. IS measurements with a wide coverage became possible in 1978 following the acquisition of a 46-m steerable antenna (MISA) that can be used with the UHF radar. Most of the early experiments were carried out by directing the antenna beam alternately 15° east and west of the magnetic meridian to secure measurements of two components of the drift velocity. Elevations of 15° and 4° were employed to cover a complete range of latitudes. Figure 1 shows the radar's primary coverage with an elevation angle of ~5° for heights below 500 km. This map is obtained from historical observational dataset. In this mode the antenna is

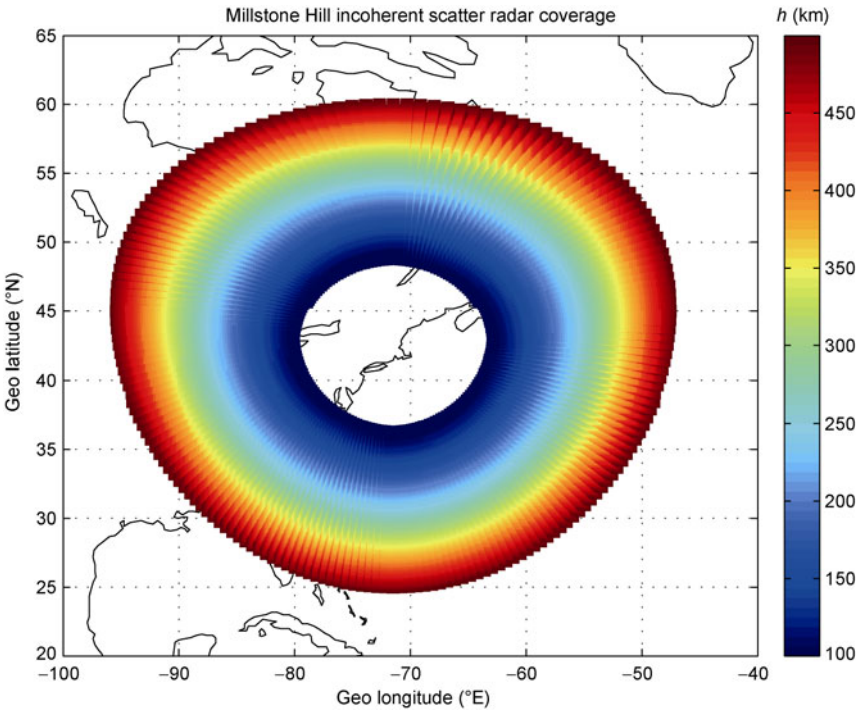

Figure 1 Millstone Hill incoherent scatter radar coverage (up to 500 km) with an elevation of ~5° for the 68-m fully steerable antenna (MISA).

moved slowly and continuously either in azimuth or in elevation and, after each MISA scan, observations are switched to the vertically directed 67-m antenna to provide local ionospheric measurements. The MISA scan rates are normally 4°–10°/min in azimuth and 2°–4°/min in elevation for the convection experiments. Radio signals are transmitted at 440 MHz by two 2.5-MW transmitters. A long-pulse of about 1280–2000 μs is often used for wide coverage experiments, yielding an altitude resolution of 35–80 km (depending on range) and a horizontal resolution of 150–300 km. Typical integration times are 30 s–5 min. Extra-wide experiments in the north direction have been extensively used to construct high-latitude convection patterns (see ref. [6] for a latest example); here we are using data from east and west directions.

3 Method

The Millstone Hill ISR is located at 288.6°E longitude. Data of interest for the present study are for the east and the west sides of the radar at 7 altitude nodes of 150, 200, 250, 300, 350, 400 and 450 km, respectively. These 14 subsets of data are basically from the radar's extreme low elevation observations so that radar signals could reach a long range while still in the F region. This elevation is ~5°. Table 1 shows data bin information of height, longitude and latitude. These position parameters are expressed as a bin median value and a standard deviation of the bin average. For ~450 km, most data were from −51°E on the east side, and −92°E on the west side, while for ~150 km, most data were from −61°E on the east side and −82°E on the west side.

We use a bit-fit method that has been extensively used for creating ISR-based empirical ionospheric models (ISRIM; see, e.g., ref. [7]). For any given bin, observational data are fitted to a model with terms of solar activity, magnetic activity, season, and local time. For the purpose of this work, we opt to a somewhat simplified approach where the solar activity term $S= s_1\times f + s_2\times f^2$, with f being F10.7, magnetic activity term $M=m_1\times ap$ with ap being the 3-h ap index, seasonal term

$$N = \sum_{k=1}^{k=2} a_k \cos\left(\frac{2\pi kd}{365}\right) + b_k \sin\left(\frac{2\pi kd}{365}\right),$$

with d being the day number of the year, and local time term

$$L = \sum_{j=1}^{j=3} c_j \cos\left(\frac{2\pi jt}{24}\right) + d_k \sin\left(\frac{2\pi jt}{24}\right),$$

with t being local time. The model parameter P (electron density, for instance) is then expressed as $P=B+S+M+N+L+C$, where B is a background term and C is a proper combination of the cross terms including $S\times N$, $S\times L$, $N\times L$, etc. It turns out that these cross terms are not all significant. We use daily F10.7 as a proxy of solar EUV flux. This is a very convenient proxy, given its accessibility for dealing with a very large dataset of long time series like this, but perhaps not the ideal one as pointed out in many prior studies (see [8–11]). However, we expect the general dependency on solar activity can be well represented because of high correlation between F10.7 and EUV shown in statistics.We have included data mostly from relatively quiet to moderate magnetic activity conditions, therefore the term M should be insignificant.

Figure 2 shows distributions of data points as a function of F10.7, day number of the year (season) and local time. Overall, data are well distributed with F10.7, but there were slightly more data for high solar activity years, with the highest mount of data centered around 175 solar flux units (sfu). More data were taken in equinox seasons than in solstice seasons, especially than in the winter solstice; more data were taken during the day especially over the evening sectors.The data distribution verse F10.7, season, and local time should not change very much with height, as data we selected are from about the same elevation of the radar beam.

It should be noted that due to the presence of buildings and woods in the radar's field of view when elevation is extremely low, there is a chance where the strength of radar's return signal differs on different beam directions. We may roughly calibrate this by equalizing Ne at 150 km for

Table 1 Geographic positions of the bins

Height (km)	Longitude (°E)	Latitude (°N)	Height (km)	Longitude (°E)	Latitude (°N)
158±14	−82±1	45±3	159±12	−61±1	45±3
197±12	−84±1	45±3	203±12	−59±2	45±3
245±14	−86±1	45±4	243±13	−56±2	46±4
300±12	−88±1	45±5	300±14	−54±2	45±5
356±12	−89±2	46±5	350±13	−54±2	47±5
397±13	−91±2	47±6	397±12	−52±2	48±6
449±12	−92±2	47±6	449±13	−51±3	48±6

Note: The three position parameters are expressed as a bin median value and a standard deviation of the bin average. The left three columns are for the observations made on the west side of Millstone Hill and the right three columns are for the east side.

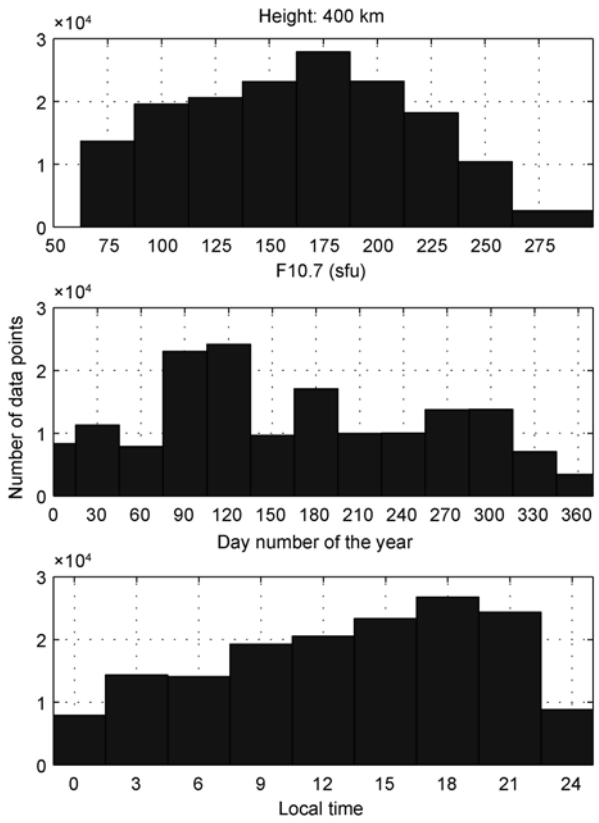

Figure 2 Data distribution for 400 km as a function of solar F10.7 index (top panel), day number of the year (middle panel), and local time (bottom panel).

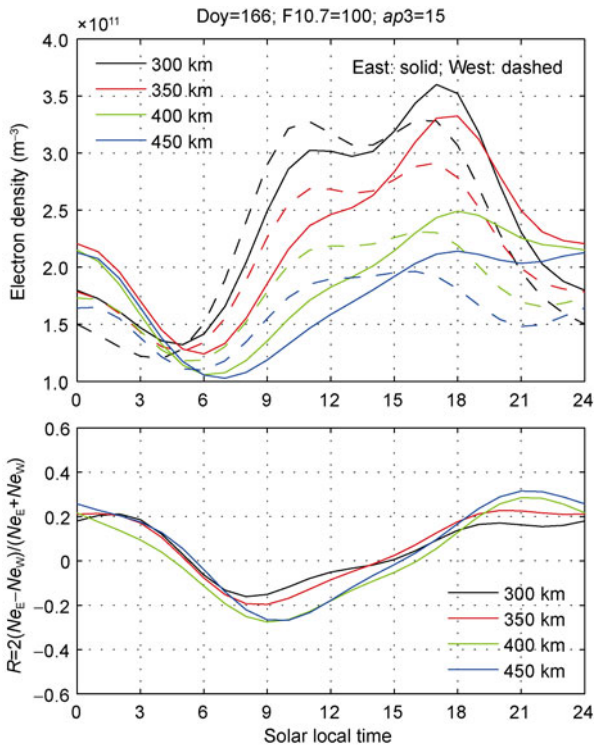

Figure 3 Local time variations of electron density for both east and west sides of the radar in summer with low-to-medium solar activity at various F region heights. The top panel shows electron density for the east side (solid lines) and the west side (dashed lines) and the bottom panel shows an east-west density ratio R, defined as $R=2(Ne_E-Ne_W)/(Ne_E+Ne_W)$, where Ne_E and Ne_W are Ne for the east and west sides, respectively.

the west and east directions and applying the calibration factor to higher altitudes. This calibration factor is on the order of 10%. As indicated in Table 1, at 150 km, since the longitudes for the east and west bins are separated by merely 21°, we can assume that there is no apparent longitudinal variation for this chemistry dominant height.

4 Result

Substantial differences in electron density Ne between the west and east sides of the radar appear in the data and change with local time, season and solar activity at various heights. In the following discussion, we present results as calculated from the model described above.

4.1 Diurnal variation

Figure 3 shows electron density at the east and west sides of the radar and their difference at F region heights. In this example for summer with low-to-medium solar activity, the Ne on the east side starts to exceed that on the west side after 1500 LT, the difference grows toward evening till the next morning before 0600 LT when the Ne on the west wide exceeds that on the east side. We may use R, defined as $R=2(Ne_E-Ne_W)/(Ne_E+Ne_W)$, similar to ref. [5] to quantify the east-west difference. Ne_E and Ne_W are electron densities on the east and the west sides. R is equivalent to a percentage difference. It can be seen that the difference maximizes, up to ~0.3 (30%) in the afternoon around 2100 LT, and minimizes in the morning, up to ~−0.3 (−30%) before 1200 LT. The difference as indicated in R tends to increase with height among these 4 height levels in the topside of the ionosphere, although their variation patterns for different heights are nearly identical. In fact, the diurnal variation pattern in R can change with season. Another case is given with similar conditions but for winter (Figure 4). Here the R variation is more symmetric to noontime such that near midday, the west Ne is highest relative to the east Ne, and vice versa for midnight. In this case, the east Ne can be higher by 60% at night than the west Ne, while the west Ne can be higher by 20% during the day.

4.2 Seasonal dependency

As indicated in the previous section for summer and winter conditions, there is a clear seasonal dependency in R. Details of the dependency can be seen in Figure 5 where R is given for 400 km at low-medium solar activity as a function of day number and local time. The positive R (i.e., $Ne_E>Ne_W$)

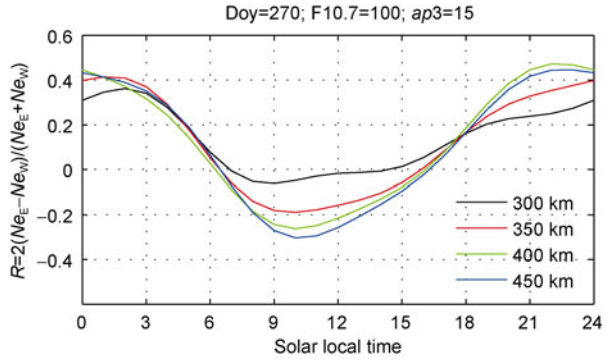

Figure 4 Diurnal variation of east-west electron density difference index *R* for winter with low-median solar activity.

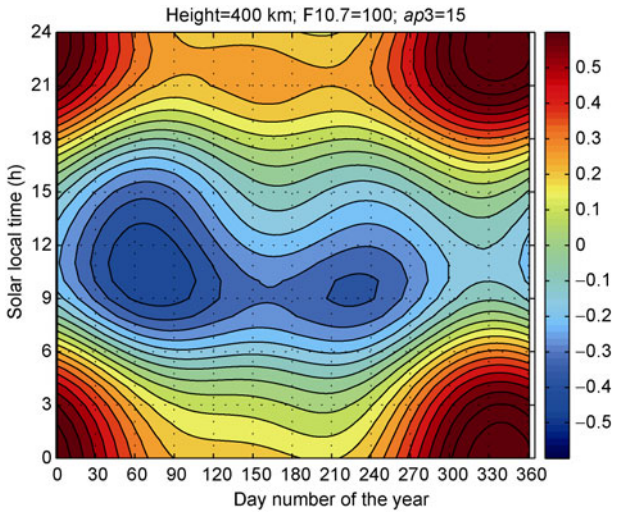

Figure 5 Contours of *R* values as a function fo day number of the year and solar local time for 400 km with low-medium solar activity.

appears to be high in winter and low in summer, with a clear annual variation. With increasing solar activity, there is a tendency for a secondary high *R* to exist right before summer (figures not to show here). The negative *R* (i.e., $Ne_E<Ne_W$), however, appears to be high in two periods, with a clear semiannual variation. These periods are the later winter-early spring period, and the later summer-early fall period. The peak is much stronger for the former time period. Such characteristics of seasonal behavior are generally true for other heights down to 300 km and for higher solar activity.

4.3 Solar activity dependency

Now we address the solar activity dependency. Since we have demonstrated previously seasonal and diurnal variations of *R*, here we pay attention only to the diurnal maximum and minimum values in *R* and observe their seasonal variations at three solar flux levels (Figure 6). The diurnal maximum *R* is when $Ne_E>Ne_W$ in the evening, and the diurnal minimum is when $Ne_E<Ne_W$ before noon. The maximum (positive) *R* is affected by the solar flux level: except for the entire summer and later spring period, the minimum (negative) *R* valueappears higher with decreasing solar activity; during the summer and later spring period, the maximum *R* value is slightly reduced with decreasing solar activity. The minimum *R* appears to behavior in a similar way the positive *R* does. The absolute value of the negative (minimum) *R* increases with decreasing solar activity, however, this is true for the period from early spring through fall. As a result,the solar activity does not seem to affect both maximum and minimum *R*s simultaneously. Indeed, the two *R*s correspond to local times of late evening and pre-noon hours (as further addressed later). Responses in the ionosphere and thermosphere to solar activity, in particular the zonal winds, can be highly time dependent.

4.4 Times of highest east-west differences

The local times of maximum and minimum east-west difference *R* are located essentially at two sectors, each of which changes smoothly with season but not much with solar activity. The time of the maximum *R* (highest positive *R*), being around 2100–2400 LT (Figure 7), occurs about 2 h earlier in summer than in winter. The time of minimum *R* (the highest negative *R*), being around 0900–1200 LT, occurs also about 2 h earlier in summer than in winter. So that the time difference between the two highest values of *R* remains a constant of 12–13 h over the course of a year.

5 Discussion

Many of our results in the east-west Ne differences shown here agree with what have been found in TEC over the US east and west coasts [5]. These include the diurnal variation pattern in *R*. Longitudinal variations over the continental US have been explained as effects of magnetic declination combined with varying zonal winds. The magnetic declination is westward (negative) on the east side of the US continent and eastward (positive) on the west side,being zero along ~−90°E longitude. The magnetic field-aligned ion drift V''_{zonal} (positive for upward drift) induced by thermospheric horizontal zonal winds U_e (positive for eastward winds), $V''_{zonal} = -U_e \sin D \cos I$, with *I* being the magnetic inclination, is either upward or downward depending on the sign of declination angle *D* and the sign of zonal winds U_e. For winds with a westward component, V''_{zonal} is upward on the west side of the zero declination longitude, and downward on the east side. The downward field-aligned drift V''_{zonal} moves the ions to lower altitudes where their recombination rate, exponentially increasing toward lower altitudes, is higher so that they are lost more quickly than they would be at higher altitudes and thus the electron density in that region is reduced. A zonal wind induced upward drift gives rise to higher *Ne* than in the downward drift regions.

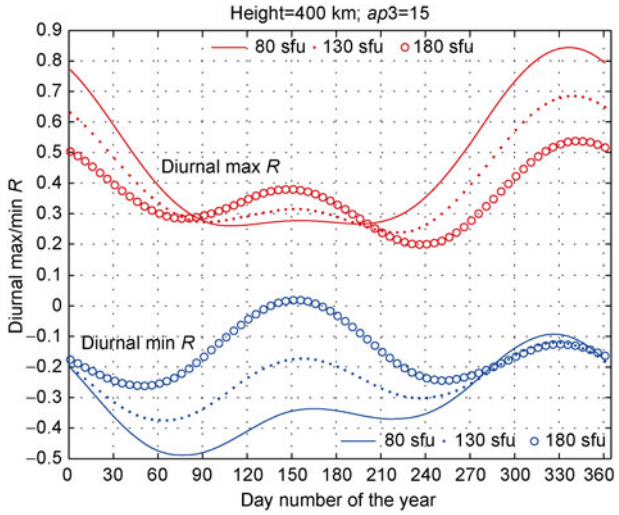

Figure 6 Seasonal and solar activity dependency of the diurnal maximum/minimum of east-west difference R. Red curves are for the diurnal maximum R (Ne_E>Ne_W), and the blue ones for the diurnal minimum R (Ne_E>Ne_W). Results are given for three levels of F10.7 solar flux units as a function of day number of the year for 400 km.

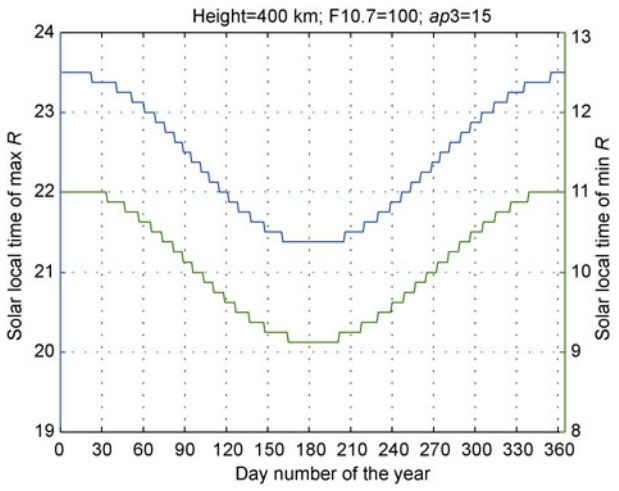

Figure 7 Time of the maximum and minimum east-west differences for 400 km at low-medium solar activity.

As a result, westward winds produce higher *Ne* on the west side of the US than on the east side. Similarly, eastward winds cause the opposite effect. Now in our case here, the longitude spans from magnetic declination zero (–90°E) to –15°—20° (–50°E—60°E). Instead of TEC, we examined Ne at the topside ionosphere where dynamics such as zonal wind effects is more important than at the bottomeside. The present results support previous conclusions that suggest a combined magnetic declination-zonal wind mechanism. Additional points can be made based on these results as described below.

5.1 Weddell-Sea anomaly

Another midlatitude phenomena called Weddell Sea anomaly (WSA) is characterized as an evening enhancement in electron density in summer. This enhancement is associated primarily with meridional winds and magnetic declination (e.g., [12–14]). Figure 3 is a summer case where we can see WSA-like variations for data from both sides. This anomaly, however, is different from the longitudinal difference that we are discussing in that: 1) The WSA is primarily an evening enhancement in Ne relative to its daytime level, while the longitudinal change here shows a diurnal course. 2) The WSA occurs in summer time; the longitudinal difference occurs persistently in all seasons, without particular (in fact, with relatively lower) preference in summer.

5.2 Zonal wind climatology

Since the east-west difference is mainly caused by the change in magnetic declination through zonal winds, the statistics shown here provides some insight into zonal wind climatology, including diurnal and seasonal variations and solar cycle dependency. In the diurnal variation, the sign change of R between negative and positive is an indication of sign change in zonal winds. The sign change in R once a day indicates the same frequency of sign change in zonal winds. It can be expected that zonal winds are very strongly eastward in the late evening when R is maximum, and westward before noon when R is minimum. In the seasonal variation, it can be also expected that the eastward wind is stronger in winter than in summer because R is larger in winter than in summer (Figure 5). For solar activity dependency, it is known that the midlatitude *Ne* decreases with decreasing solar activity; as a result, winds tend to be stronger due to weaker ion drag. Therefore the stronger zonal wind can give rise to larger $|R|$ for lower solar activity (Figure 6).

Zonal wind climatology over Millstone Hill has been published based on FPI measurements for a full solar cycle in 1989–2001 [15]. It was indicated that the eastward wind reach maximum before but close to midnight; the eastward wind in the evening is highest in winter; the eastward wind speed tends to be enhanced toward low solar activity, in particular, in winter. All these results are perfectly consistent with the expectation, which is addressed in the previous paragraph, based on the east-west *Ne* differences.

The directional reversal/change in declination causes a large difference in *Ne* through the zonal wind induced ion drift, and therefore it might be feasible to derive zonal wind information based on corresponding electron density. For this purpose, simple numerical models that involve main midlatitude chemical and physical processes can be easily implemented to establish a quantitative relationship between zonal winds and the resultant longitudinal difference in *Ne*. In fact, decades ago similar ideas for deducing equivalent meridional winds from the height of the F2-peak were introduced and widely used (see early papers in refs. [16–19]).

5.3 Longitudinal variations for other sectors

Similar longitudinal variations at a given local time may exist in European and Asian sectors. However, the magnitudes of these predicted variations can be different from those for the America sectors due to different magnetic field configurations and the fact that the distance to the magnetic pole varies with longitude [4]. It was noted [20] that there was a significant difference in foF2 between a pair of Chinese midlatitude stations with a 40° longitude separationbut similar latitudes: Unumuqi and Changchun. Over the subcontinent China, the zero magnetic declination for midlatitudes is 90°E–100°E, close to but on the west side of the longitude line of geographic center of China. Unumuqi is on the west side with positive declination and Changchun is on the east side with negative declination. Their study showed the diurnal variation of the west-east (Unumuqi-Changchun) difference in foF2. This difference is exactly the same as shown here and in ref. [5] Further indication of the longitudinal difference between the two stations was shown in the spread-F occurrence [21]. With proper zonal wind information, it will be possible to explain the observed differences in electron density over the two stations in terms of magnetic declination and zonal winds. This topic deserves a more comprehensive investigation in the future using a similar analysis technique for data from the Chinese subcontinent.

6 Summary

A substantial difference in the US east-west coast electron density has recently been found for given local times, and varies with local time. This longitudinal difference is due to the combined magnetic declination-zonal wind effect. Our current study provides strong supporting evidence for the phenomena and plausible mechanism from a totally independent data source: incoherent scatter radar long-term observations over Millstone Hill. The extra-wide coverage of the radar allows for a study of the ionospheric differences on east and west sides of the radar. The longitudinal separation at 400 km is 40° and the data span 3 solar cycles during years 1978–2010. We have been able to address the diurnal and seasonal variations and solar cycle dependency of electron density differences between both sides at high F region heights. These results can be summarized as the following.

1) The east-west difference in *Ne* is significant and can be up to 60%. It varies over the course of the day, being positive (East side *Ne* > West side *Ne*) in the late evening and negative (West side *Ne* > East side *Ne*) in the pre-noon.

2) The east-west difference exists throughout the year. The positive (relative) difference is most pronounced in winter; the negative (relative) difference is most pronounced in early spring and later summer.

3) The east-west difference depends on solar activity. The positive difference enhances with decreasing solar activity for more than half a year, mostly in winter and fall, but not for the spring-later summer period; almost during the same spring-later summer time period, the negative difference also enhances with decreasing solar activity. The enhancements of the positive and negative differences do not occur simultaneously.

4) The times of largest positive and largest negative east-west differences in *Ne*, being in the late evening and pre-noon hours, respectively, are earlier in summer and later in winter. The two times differ by 12–13 h constantly throughout the year.

5) Variations at different heights from 300–450 km are similar.

Zonal wind climatology over Millstone Hill is perfectly consistent with what is expected based on the electron density difference between the east and west sides of the site. This study indicates that longitudinal variations for some regions in ionospheric electron density contain critical information on thermospheric zonal winds. The declination-zonal wind mechanism can be used to derive zonal winds, in addition to understanding ionospheric variations in other longitude sectors.

This work was supported by the National Natural Science Foundation of China (Grant No. 40890164) and the US National Science Foundation under Cooperative Agreements (Grant Nos. ATM-0733510 and ATM-6920184). We thank the members of the MIT Haystack Observatory for maintaining the Madrigal Database. We are indebted to Prof. Xiao Zuo for his encouragement in preparing this paper, and to Drs. Zhang Manlian and Zhang Beichen for their hospitality and help during recent visits to China by one of the authors (SRZ).

1 Sagawa E, Immel T J, Frey H U, et al. Longitudinal structure of the equatorial anomaly in the nighttime ionosphere observed by IMAGE/FUV. J Geophys Res, 2005, 110: A11302
2 Immel T J, Sagawa E, England S L, et al. Control of equatorial ionospheric morphology by atmospheric tides. Geophys Res Lett, 2006, 33: L15108
3 England S L, Immel T J, Huba J D, et al. Modeling of multiple effects of atmospheric tides on the ionosphere: An examination of possible coupling mechanisms responsible for the longitudinal structure of the equatorial ionosphere. J Geophys Res, 2010, 115: A05308
4 Rishbeth H. How the thermospheric circulation affects the ionospheric F2-layer. J Atmos Sol-TerrPhys, 1998, 60: 1385–1402
5 Zhang S R, Foster J C, Coster A J, et al. East-west coast differences in total electron content over the continental US. Geophys Res Lett, 2011, 38: L19101
6 Zhang S R, Holt J M, McReady M. High latitude convection model based on long-term incoherent scatter radar observations in North America. J Atmos Sol-TerrPhys, 2007, 69: 1273–1291
7 Zhang S R, Holt J M. Ionospheric climatology and variability from long-term and multiple incoherent scatter radar observations: climatology in Eastern American Sector. J Geophys Res, 2007, 112: A06328
8 Balan N, Bailey G J, Jenkins B, et al. Variations of ionospheric ioni-

zation and related solar fluxes during an intense solar cycle. J Geophys Res, 1994, 99: 2243–2253
9 Richards P G, Torr D G, Reinisch B W, et al. F2 peak electron density at Millstone Hill and Hobart:Comparison of theory and measurement at solar maximum. J Geophys Res, 1994, 99: 15005–15016
10 Liu L, Wan W, Ning B. Statistical modeling of ionospheric foF2 over Wuhan. Radio Sci, 2004, 39: RS2013, doi:10.1029/2003RS003005
11 Lei J, Liu L, Wan W, et al. Variations of eletrondensity based on long-term incoherent scatter radar and ionosonde measurements over Millstone Hill. Radio Sci, 2005, 40: RS2008
12 Luan X, Wang W, Burns A, et al. Midlatitude nighttime enhancement in F region electron density from global COSMIC measurements under solarminimum winter condition. J Geophys Res, 2008, 113: A09319
13 Lin C H, Liu C H, Liu J Y, et al. Mid-latitude summer nighttime anomaly of the ionospheric electron density observed by FORMOSAT-3/COSMIC. J Geophys Res, 2010, 115: A03308
14 Chen C H, Huba J D, Saito A, et al. Theoretical study of the ionospheric Weddell Sea Anomaly using SAMI2. J Geophys Res, 2011, 116: A04305
15 Emmert J T, Fejer B J, Sipler D P. Climatology and latitudinal gradients of quiet time thermospheric neutral winds over Millstone Hill from Fabry-Perot interferometer measurements. J Geophys Res, 2003, 108: 1196
16 Rishbeth H, Ganguly S, Walker J C G. Field-aligned and field-perpendicularvelocities in the ionospheric F2-layer. J Atmos Terr Phys, 1978, 40: 767–784
17 Buonsanto M J. Seasonal variations of day-time ionisation flows inferred from a comparison of calculated and observed NmF2. J Atmos Terr Phys, 1986, 48: 365–373
18 Zhang S R, Su Y, Huang X. Plasma drifts at the ionospheric F2 peak (in Chinese). ACTA Chin J Space Sci, 1992, 13: 298–304
19 Zhang S R, Huang X Y. Neutral wind-induced F region movements under the coupling of ionosphere-thermosphere (in Chinese). ACTA Chin J Space Sci, 1995, 15: 105–118
20 Wu J, Cao Z H, Quan Q H. Observations of thelongitude effects in the mid-latitude ionospheric F regionand comparisons with models (in Chinese). ACTA Chin J Space Sci, 1998, 18: 132–140
21 Huang W Q, Xiao Z, Xiao S G, et al. Case study of apparentlongitudinal differences of spread F occurrence for two midlatitude stations. Radio Sci, 2011, 46: RS1015